Pressure-induced quantum critical behavior and magnetic order in $YbNi_3Ga_9$ with a chiral crystal structure: ac calorimetric measurements up to 12 GPa

Kazunori Umeo,[1] Takumi Otaki,[2] Yudai Arai,[2] Shigeo Ohara,[3] and Toshiro Takabatake[2]

[1]*Cryogenics and Instrumental Analysis Division, N-BARD, Hiroshima University, Higashi-Hiroshima, 739-8526, Japan*

[2]*Department of Quantum Matter, Graduate School of Advanced Sciences of Matter, Hiroshima University, Higashi-Hiroshima 739-8530, Japan*

[3]*Department of Engineering Physics, Electronics and Mechanics, Graduate School of Engineering, Nagoya Institute of Technology, Nagoya 466-8555, Japan*

(Received 9 April 2018; revised manuscript received 6 July 2018; published 23 July 2018)

The chiral compound $YbNi_3Ga_9$ with a trigonal structure, which is a valence fluctuating material at ambient pressure, undergoes a magnetic order under pressure above P_c of 9 GPa. We have studied the temperature-pressure-magnetic-field phase diagrams of this compound by ac calorimetric measurements under pressures P up to 12 GPa. The specific heat C divided by temperature T, C/T, markedly increases with applying pressure up to P_c. At 8.6 GPa, just below P_c, C/T exhibits $-\ln T$ dependence in the temperature range 2–9 K. At $T < 1.5$ K, C/T is saturated to a large value 1 J/K^2 mol, i.e., heavy Fermi-liquid behavior. At $P = 9.3$ GPa, just above P_c, a broad maximum in C/T appears at 1.6 K, indicating the onset of the magnetic order. With increasing P further, the maximum shifts to a higher temperature and transforms to a sharp λ-type peak at 5 K for $P \geqslant 11$ GPa. By using the temperature, pressure, and magnetic field B dependences of the specific-heat data $C(T, P, B)$ obtained under $B \perp c$ and $B \| c$, we have constructed B-T phase diagrams at each P value. Another field-induced ordered phase appears in the diagrams only for $B \perp c$ at $P \geqslant 11$ GPa. The origin of this induced phase is discussed in relation to the chiral soliton lattice and the skyrmion lattice reported for chiral magnets.

DOI: 10.1103/PhysRevB.98.024420

I. INTRODUCTION

Recently, chiral magnets such as $CrNb_3S_6$ [1], MnSi [2], and FeGe [3] have attracted a great deal of interest. In chiral magnets, novel magnetic structures such as a chiral soliton lattice (CSL) and skyrmion lattice are caused by the asymmetric spin interaction, the so-called Dzyaloshinskii-Moriya interaction. The CSL is a type of superlattice structure that consists of a periodic helical spin texture [1]. Most chiral magnets have been based on 3d-transition elements thus far. Recently, chiral magnets based on rare-earth elements such as Yb or Eu have been synthesized, for which unusual magnetic properties have been reported [4,5].

Studies of Yb-based intermetallic compounds have enriched strongly correlated electron phenomena such as quantum critical phenomena, unconventional superconductivity, and anomalous magnetic orders [6–8]. For example, application of pressures P can tune the ground state continuously from a paramagnetic state to a magnetically ordered state through a quantum critical point [9]. In the vicinity of the critical point, physical properties display an unusual power law or logarithmic temperature dependences, the so-called non-Fermi-liquid (NFL) behaviors [10]. The NFL behaviors for some Yb compounds are explained by the self-consistent renormalization theory [11,12]. However, the NFL behaviors in $YbRh_2Si_2$ [13] and β-$YbAlB_4$ [7,14] cannot be described by the spin-fluctuation theory but are explained in terms of a critical valence fluctuation of Yb ions [15].

The compounds $YbNi_3X_9$ (X = Al and Ga) are potential candidates exhibiting chiral magnetic structures as well as quantum critical phenomena [4,16–19]. The two compounds crystallize in the trigonal $ErNi_3Al_9$-type structure with space group $R32$. $YbNi_3Al_9$ undergoes a chiral helical magnetic ordering transition at $T_M = 3.4$ K [4,16]. Neutron diffraction measurements revealed that the magnetic structure below T_M is helical, characterized by the magnetic propagation vector $q = (0\,0\,0.8)$ [4]. By applying magnetic fields B of 0.1 T along the a axis (perpendicular to the helical axis, i.e., the c axis), the helical state changes into a forced ferromagnetic state [4,16]. By substituting 6% of Cu for Ni in $YbNi_3Al_9$, the value of the metamagnetic field B_c increases up to 1 T, and the magnetization curve below $T_M = 6.4$ K exhibits a downward convex curve, a characteristic feature of CSL [17,18]. The specific heat $C(T)$ of $Yb(Ni_{0.94}Cu_{0.06})_3Al_9$ shows a sharp peak at T_M under magnetic fields of $0 < B < B_c$ [18]. Recent resonant x-ray diffraction measurements have revealed that the CSL is realized in the field range $B < B_c$ [19]. In the CSL, Yb spins form a superlattice composed of commensurate forced-ferromagnetic domains periodically partitioned by incommensurate 2π rotation of spins [1].

$YbNi_3Ga_9$, on the other hand, is an intermediate-valence system with a Kondo temperature of $T_K = 570$ K [4,20]. A magnetic order was expected to occur when high pressures are applied on this compound. Indeed, a magnetic order above $P_c = 9$ GPa was inferred from the electrical resistivity ρ and ac magnetic susceptibility χ_{ac} measurements [21]. Under $P = P_c$, $\rho(T)$ at low temperatures exhibits a linear-temperature dependence, i.e., NFL behavior. At 8.5 GPa, just below P_c, the field dependence of $\chi_{ac}(B \| a)$ indicated a hysteretic anomaly at 0.7 T, which was attributed to a first-order metamagnetic transition. This transition was discussed by means of the

 ©2018 American Physical Society

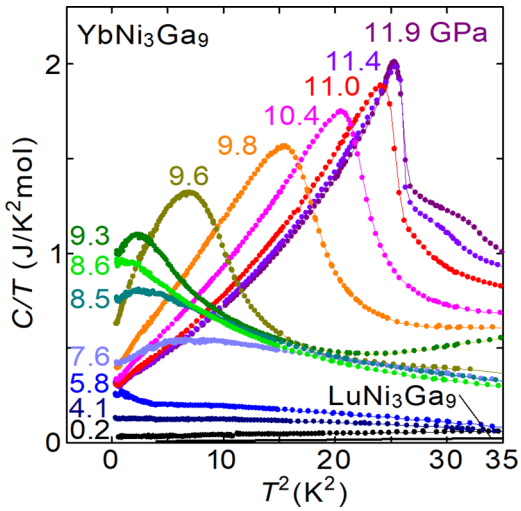

FIG. 1. Specific heat divided by temperature C/T vs T^2 for $YbNi_3Ga_9$ under various pressures. The solid line indicates C/T of $LuNi_3Ga_9$ at $P = 0$ [4].

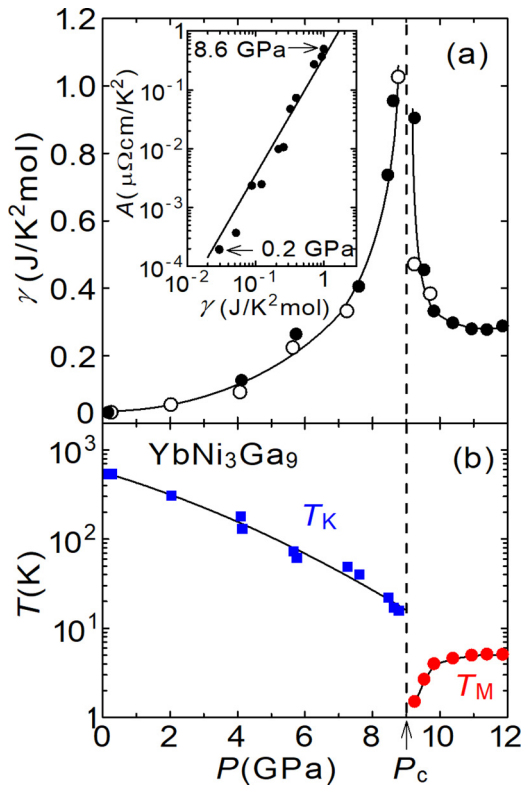

FIG. 2. Pressure dependences of (a) Sommerfeld coefficient γ and (b) Kondo temperature T_K and magnetic ordering temperature T_M for $YbNi_3Ga_9$. The inset in (a) shows the logarithmic plot of the coefficient A for the T^2 dependence of the resistivity [21] and the Sommerfeld coefficient γ under various pressures. The solid line represents the generalized Kadowaki-Woods ratio $A\gamma^{-2}[N(N-1)/2]^{-1}$ with the degeneracy $N = 8$ [24].

critical valence fluctuation theory [15]. Because quantum critical phenomena have been reported only for the resistivity, the magnetic and thermodynamic properties of the pressure-induced magnetic order above P_c remain to be investigated.

In this paper, we report the specific-heat measurements of $YbNi_3Ga_9$ under pressures up to 12 GPa and magnetic fields up to 8 T applied parallel and perpendicular to the c axis. We discuss the quantum critical phenomena in the specific heat near P_c. Furthermore, we show and discuss the B-T phase diagrams above P_c constructed by using $C(T, P, B)$ data obtained under $B \perp c$ and $B \| c$.

II. EXPERIMENTAL PROCEDURES

Single-crystalline samples of $YbNi_3Ga_9$ were grown by the Ga self-flux technique [4]. The measurement of the specific heat C was performed by the ac method in the ranges of pressure, temperature, and magnetic field, $P < 12$ GPa, $0.5 < T < 10$ K, and $0 < B < 8$ T, respectively. Thereby, we combined a Bridgman anvil cell, a ^{3}He cryostat, and an 8-T superconducting magnet [22]. A sample of 1.50 mg was wrapped with 4.83 mg of indium foil, which plays the role of a pressure transmitting medium. The wrapped sample was packed in a Cu-Be gasket (6.33 mg). Two chip resistors for the thermometer and the heater were mounted on the outer flange of the gasket. Because the thermometer is free from pressure, it was not necessary to be calibrated under different pressures. The pressure was estimated by the pressure dependence of the superconducting transition temperature of the In foil. The details of the experimental setup were described in Ref. [22].

III. RESULTS AND DISCUSSION

A. Quantum critical phenomena in the specific heat near P_c

Figure 1 shows the specific heat C divided by temperature T, C/T, under various pressures as a function of T^2. With increasing pressure, the value of C/T at low temperature increases and reaches a large value of 1 J/K^2 mol at 8.6 GPa. At $P = 9.3$ GPa, just above P_c, a broad maximum of C/T appears at 1.6 K, which is the manifestation of a magnetic order, as will be noted below. With increasing pressure, the maximum of C/T shifts to higher temperatures and grows to a λ-type peak at $T_M = 5$ K for $P > 11$ GPa. The peak temperature agrees with T_M in the resistivity data at $P = 11$ GPa [21].

First, to assess the pressure dependence of the Sommerfeld coefficient γ, we analyze the data of C/T by dividing into three contributions: the electronic, magnetic, and phonon contributions, $C = \gamma T + C_{mag} + C_{ph}$. Because $C_{mag} = 0$ for $P < P_c$, the γ values are estimated by an extrapolation of the linear portion of the C/T vs T^2 curve to 0 K. For $P > P_c$ and $T < T_M$, where C_{mag} is given by αT^n where α and $n (1 \leqslant n \leqslant 3)$ [23] are constant, we evaluate the γ values by fitting with $C = \gamma T + \alpha T^n + \beta T^3$ to the data.

The γ values are plotted in Fig. 2(a) as a function of pressure. For $P = 0.2$ GPa, γ of 30 mJ/K^2 mol agrees with the reported value for $P = 0$ [4]. With increasing pressure up to 8.6 GPa, the γ value increases to 1 J/K^2 mol. Note that the γ value is related to the T^2 coefficient A of the resistivity through the generalized Kadowaki-Woods ratio $A\gamma^{-2}[N(N-1)/2]^{-1}$ with an orbital degeneracy N [24]. The inset of Fig. 2(a) shows a double logarithmic plot of γ and A, where A at various pressures was estimated using the resistivity data reported in Ref. [21]. These data sets of γ and A are close to the straight

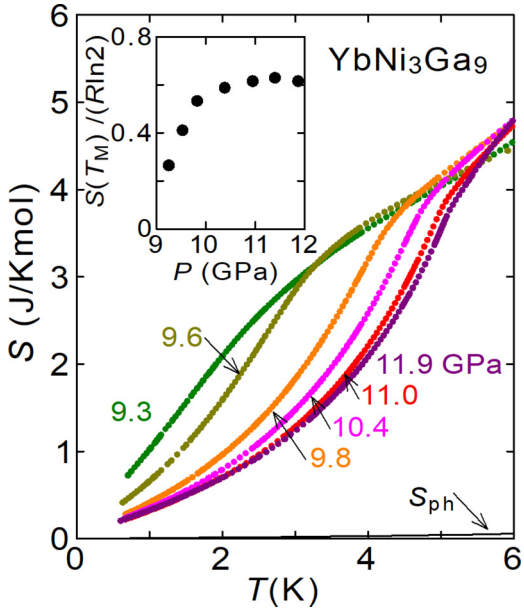

FIG. 3. Temperature dependence of the entropy S for $YbNi_3Ga_9$ at various pressures above P_c. The thin line at the bottom indicates $S(T)$ for $LuNi_3Ga_9$ [4], which represents the phonon contribution S_{ph}. The inset shows the pressure dependence of S at T_M.

line expected by the generalized Kadowaki-Woods ratio for $N = 8$.

Now, we evaluate T_K for $P < P_c$ from the γ value using the expression $T_K = R(N-1)\pi^2 W(N)/(3N\gamma)$, where R and $W(N)$ are the gas constant and the Wilson number, respectively [25–27]. Here, we adopt N as 8 according to the above result. The obtained T_K is plotted in Fig. 2(b) as a function of pressure. As pressure is increased up to 8.6 GPa, the value of T_K decreases down to 16 K, which is still a rather high temperature even in the vicinity of P_c. As shown in Fig. 2(b), for $P > P_c$, T_M rapidly rises with pressure and reaches 5 K at 11 GPa, whereas it does not change for $P > 11$ GPa.

Figure 3 shows the temperature dependence of the entropy S of $YbNi_3Ga_9$ at various pressures for $P > P_c$, which is derived from the C/T data in Fig. 1. The entropy S has two contributions from $4f$ electrons S_{4f} and phonons S_{ph}. The value of S_{ph} for $P = 0$ was estimated using the phonon part of $C(T)$ of $LuNi_3Ga_9$. Because the magnitude of S_{ph} is negligible as shown in Fig. 3, the value of S for $YbNi_3Ga_9$ is solely attributed to S_{4f}. As shown in the inset, $S(T_M)$ for $P > 11$ GPa is saturated to $0.6R\ln 2$, which is a value smaller than $0.7R\ln 2$ for the isostructural compound of $YbNi_3Al_9$ at $P = 0$ [4,16]. The smaller $S(T_M)$ for $YbNi_3Ga_9$ may be related to the higher $T_K = 16$ K even at P_c compared with $T_K = 2.7$ K for $YbNi_3Al_9$ [4].

To examine the quantum critical behavior in $C(T)$ near P_c, we plot C/T vs $\ln T$ in Fig. 4. As pressure approaches P_c, the temperature range following the form of $C/T \propto -\ln T$ becomes wider, i.e., 2–9 K for 8.6 GPa. At $T < 1.5$ K, however, C/T becomes constant, which contradicts the $-\ln T$ dependence expected near the quantum critical point from the mode-coupling theory for critical valence fluctuations [28]. A finer tuning of the pressure and magnetic field may be needed to observe the critical behavior down to zero temperature.

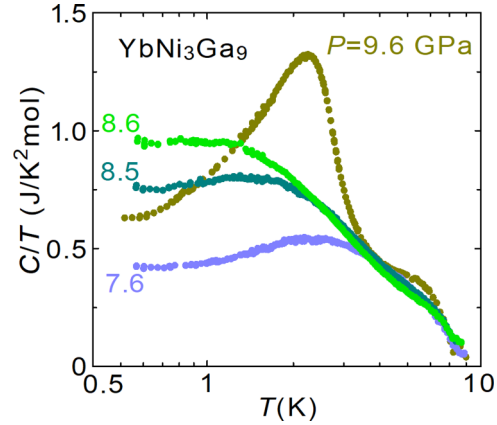

FIG. 4. Logarithmic temperature dependence of C/T under various pressures near P_c for $YbNi_3Ga_9$.

We have measured the field dependence of the specific heat at various constant temperatures, in order to investigate the field-induced first-order metamagnetic transition near $B\perp c = 0.7$ T that was observed in $\chi_{ac}(B\perp c)$ at $P = 8.5$ GPa $< P_c$ [21]. As shown in Fig. 5, C/T at 0.8 K for $P = 8.5$ GPa exhibits a maximum at $B_m = 0.9$ T. With increasing temperature, the maximum slightly shifts to low fields and becomes broader. As the temperature is increased above 2.3 K, the maximum is smeared out. At a slightly higher pressure of 8.6 GPa, the value of B_m decreased down to 0.5 T. These values of B_m agree with the values observed in $\chi_{ac}(B\perp c)$ measurements. Thus, the maxima in C/T are attributed to the metamagnetic transition. However, any hysteresis in $C(B)$ indicative of the first-order transition has not been observed.

B. Magnetic phase diagrams for $P > P_c$

To gain insight into the pressure-induced magnetic phase for $P > P_c$, we have measured the specific heat under magnetic fields for two configurations, $B\perp c$ and $B\|c$, denoted by $B^\perp$ and $B^\|$, respectively, as shown in Figs. 6 and 7.

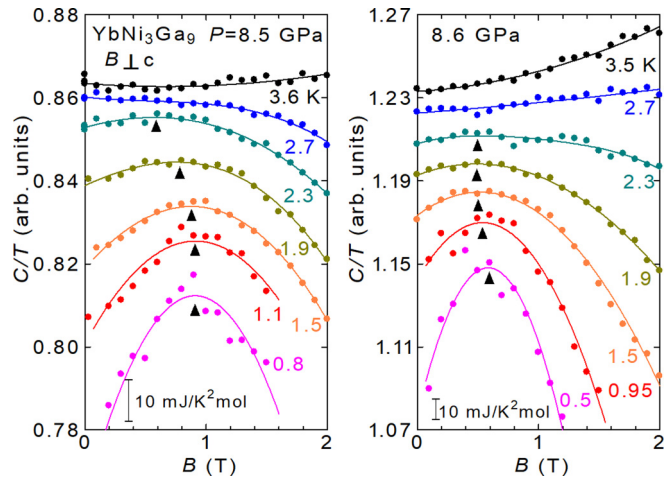

FIG. 5. Specific heat divided by temperature C/T for $YbNi_3Ga_9$ as a function of magnetic field $B\perp c$ at various constant temperatures under $P = 8.5$ (left) and 8.6 GPa (right) below P_c. Solid lines are guides to the eye.

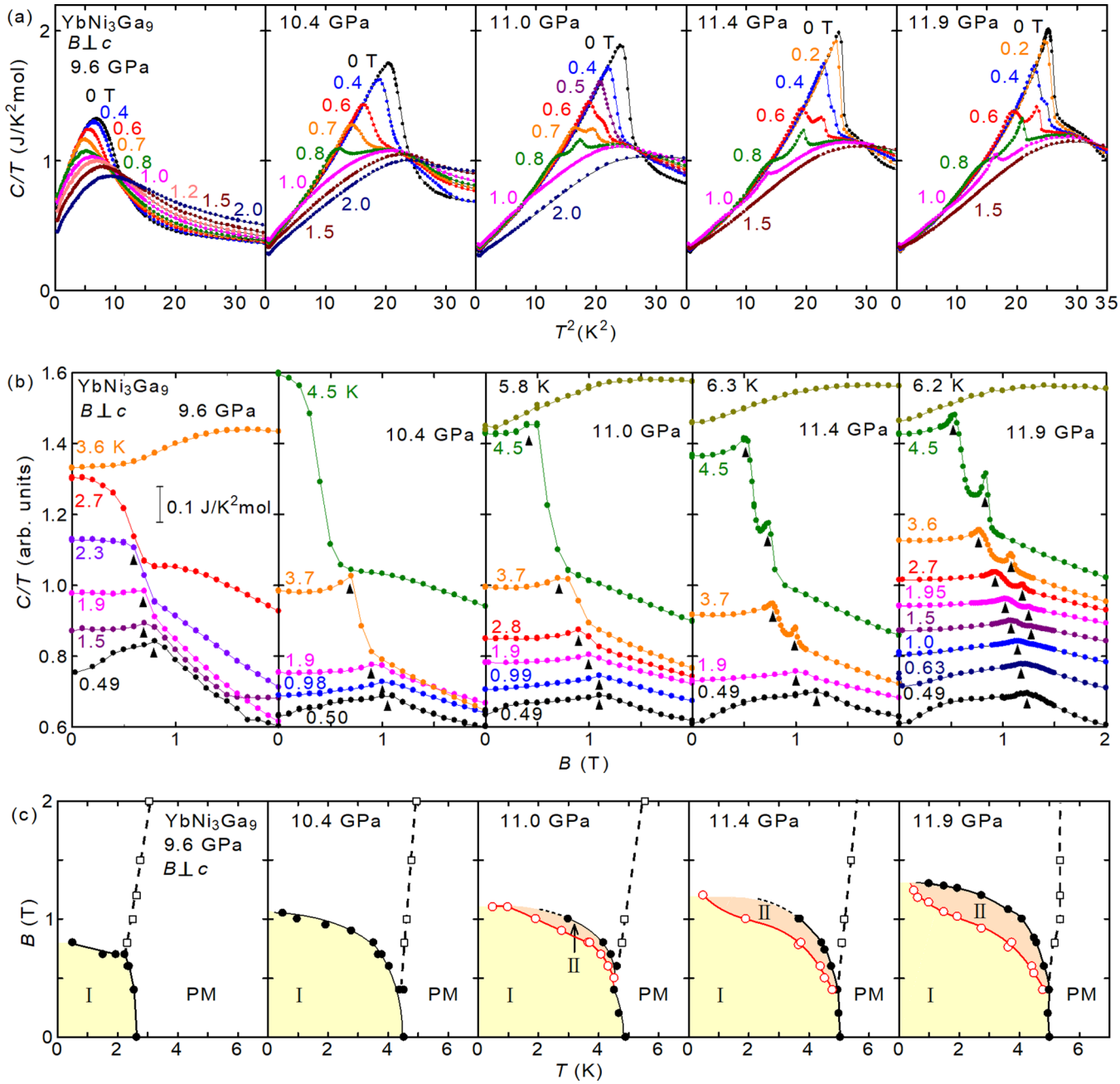

FIG. 6. (a) Specific heat divided by temperature C/T vs T^2 for $YbNi_3Ga_9$ under magnetic fields $B\perp c$ up to 2 T at various pressures above P_c. (b) Magnetic field dependence of C/T at various temperatures, in which an offset is added for clarity. (c) B-T phase diagrams at various pressures determined by specific-heat data shown in (a) and (b), where the open square denotes the peak temperature in C/T in the paramagnetic phase.

For $B\perp c$, the T and B dependences of C/T are represented in Figs. 6(a) and 6(b), respectively. First, we focus on the data at $P = 9.6$ GPa. In Fig. 6(a), the peak of C/T vs T^2 shifts to lower temperatures with increasing $B^{\perp}$ up to 0.8 T. For $B^{\perp} > 1$ T, the peak of C/T vs T^2 changes to a broad maximum and shifts to higher temperatures. The broad maximum is attributed to the Schottky-type thermal excitations between the two Zeeman-split energy levels of the ground-state doublet. As shown in Fig. 6(b), the peak and sharp drop of C/T vs B appear for $T < 2.7$ K. In the B-T phase diagram in Fig. 6(c), which is constructed by using the T and B dependences of the specific-heat data, the magnetically ordered phase noted as phase I ends at the critical fields $B_c = 0.8$ T. The value of B_c increases with increasing pressure. For $P \geqslant 11$ GPa, the peak of C/T vs T^2 splits into two peaks in the field range $0.4 \leqslant B^{\perp} \leqslant 1$ T. Similar splitting is also observed in the B dependence of C/T vs T in Fig. 6(b) for $P \geqslant 11.4$ GPa. These splits suggest another field-induced ordered phase, which is denoted as phase II in Fig. 6(c).

For $B\|c$, the features of T and B dependences of C/T and $P < 11$ GPa shown in Figs. 7(a) and 7(b) are similar to those for $B\perp c$. However, the value of $B_c = 1$ T at $P = 9.6$ GPa in

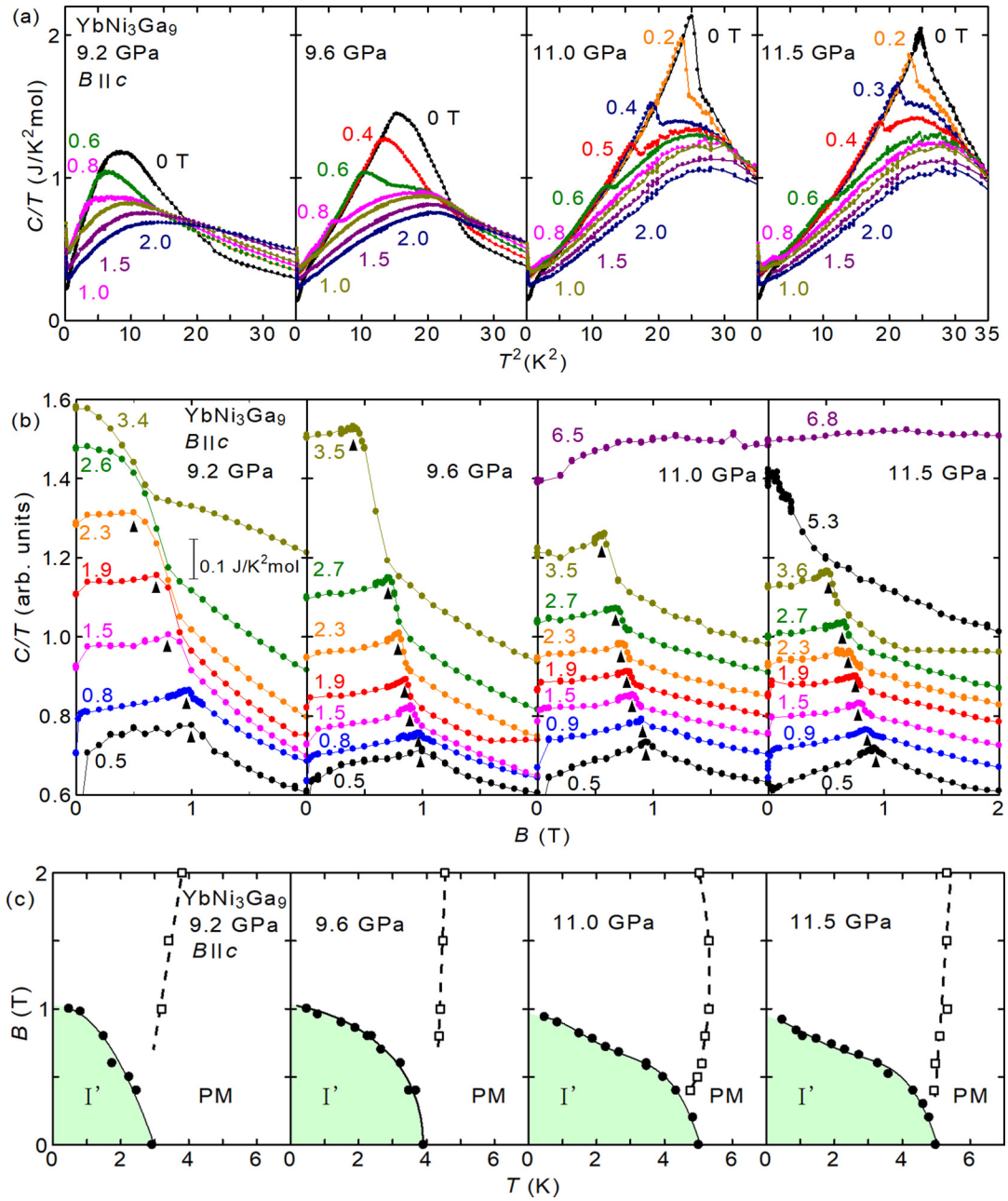

FIG. 7. (a) Specific heat divided by temperature C/T vs T^2 of $YbNi_3Ga_9$ under magnetic fields $B\|c$ up to 2 T at various pressures above P_c. (b) Magnetic field dependence of C/T at various temperatures, in which an offset is added for clarity. (c) B-T phase diagrams at various pressures determined by specific-heat data shown in (a) and (b), where the open square denotes the peak temperature in C/T in the paramagnetic phase.

Fig. 7(c) is close to 0.8 T for $B\perp c$ in Fig. 6(c). With increasing pressure, the value of B_c decreases slightly in contrast with the increase for $B\perp c$. It should be noted that, as shown in Fig. 7(c), the phase II found for $B\perp c$ does not appear for $B\|c$ up to 11.5 GPa.

First, we discuss the magnetic order of $YbNi_3Ga_9$ under various pressures. Although our specific-heat data solely do not decide the magnetic structure, we propose possible magnetic orders in terms of the magnetic structures in the compounds with related crystal structures. The crystal structure of $YbNi_3Ga_9$ seems to be unchanged under certain pressures because no feature of a structural phase transition has been found in our specific-heat data nor the resistivity data in Ref. [21]. Even if the crystal structure was changed under certain pressures, we expect the crystal symmetry to keep chirality. Let us compare the obtained B-T phase diagrams of $YbNi_3Ga_9$ under various pressures with that of $Yb(Ni_{1-x}Cu_x)_3Al_9$ at $P = 0$ in terms of T_M and B_c. We denote B_c for $B\perp c$ and $B\|c$ by $B_c^{\perp}$ and $B_c^{\|}$, respectively. The value of $T_M = 5$ K for $YbNi_3Ga_9$ at $P = 11.9$ GPa is closer to $T_M = 6.4$ K for $Yb(Ni_{0.94}Cu_{0.06})_3Al_9$ than $T_M = 3.4$ K for $YbNi_3Al_9$. For $YbNi_3Ga_9$ at $P = 11.9$ GPa, the anisotropy between $B_c^{\perp} = 1.2$ T and $B_c^{\|} = 0.9$ T is weak. This weak anisotropy is similar to the case for $Yb(Ni_{0.94}Cu_{0.06})_3Al_9$ with

$B_c^{\perp} = B_c^{\parallel} = 1$ T, rather than that for $YbNi_3Al_9$ with $B_c^{\perp} = 0.1$ T and $B_c^{\parallel} = 1.8$ T [18]. These similarities in the magnetic phase diagrams between $YbNi_3Ga_9$ under certain pressures and $Yb(Ni_{0.94}Cu_{0.06})_3Al_9$ under ambient pressure suggest that the CSL emerges in the pressure-induced magnetic phase of $YbNi_3Ga_9$ under magnetic fields for $B \perp c$.

Next, let us discuss the nature of the phase II of $YbNi_3Ga_9$ in Fig. 6(c), which appears for $B \perp c$ and $P \geqslant 11$ GPa. It is noteworthy that such a field-induced phase has not been observed in $Yb(Ni_{0.94}Cu_{0.06})_3Al_9$. A recent theory on a monoaxial helimagnet has predicted that a highly nonlinear CSL (HNL-CSL) appears close to the phase boundary from CSL to the paramagnetic (PM) phase at high magnetic fields [29]. Actually, the magnetization measurements for $CrNb_3S_6$ revealed that the CSL state consists of CSL-1 with a dominant helical texture and a poor ferromagnetic array and CSL-2 (HNL-CSL) with a large ferromagnetic array [30]. However, the phase of CSL-2 is not a thermodynamic phase, because the transformation from CSL-1 to CSL-2 is a sort of crossover rather than a phase transition. The phase II in $YbNi_3Ga_9$, however, is thought to be a thermodynamic phase, in view of the obvious peak in both C/T vs T^2 and C/T vs B as shown in Fig. 6.

Another possibility of the phase II is a skyrmion lattice [2]. In the B-T phase diagram of $YbNi_3Ga_9$ for $B \perp c$ and $P = 11.9$ GPa, the phase II in Fig. 6(c) appears near the phase boundary between the phase I and field-induced ferromagnetic phase. This feature is similar to the skyrmion lattice phase found in MnSi, FeGe, and Cu_2OSeO_3 [2] and the A phase in EuPtSi [5]. The specific heat of MnSi under magnetic fields exhibits two clearly distinguished peaks [31], an observation that has proved the skyrmion lattice in MnSi to be a thermodynamic phase. The crystal symmetry of $YbNi_3Ga_9$ itself allows the formation of a skyrmion lattice [32], whereas the absence of a ferromagnetic nature seems to be unfavorable. In order to determine the magnetic structure of the field-induced phase in $YbNi_3Ga_9$, magnetization and neutron diffraction measurements for $P \geqslant 11$ GPa are highly desirable.

IV. SUMMARY

In the present work, we have studied the pressure-induced quantum critical behavior and magnetic ordered phase in the chiral compound $YbNi_3Ga_9$ by the measurements of the specific heat C under pressures up to 12 GPa and magnetic fields up to 8 T. First, C/T shows a NFL behavior $C/T \propto -\ln T$ near P_c and the γ value is increased to a large value of 1 J/K^2 mol. Furthermore, field-induced maxima appear in C/T vs $B \perp c$, which are attributed to a metamagnetic transition. Second, we constructed B-T phase diagrams for $B \perp c$ and $B \| c$ at various constant pressures from the $C(T, P)$ data. The magnetic phase diagrams for $YbNi_3Ga_9$ under pressures resemble those for $Yb(Ni_{0.94}Cu_{0.06})_3Al_9$ with the CSL, suggesting the emergence of CSL in $YbNi_3Ga_9$ for $B \perp c$. Furthermore, we found another field-induced ordered phase for $B \perp c$ and $P \geqslant 11$ GPa. The multiple phases found in this system would promote studies of chiral magnets based on rare-earth ions.

ACKNOWLEDGMENTS

We acknowledge valuable discussions with K. Inoue, Y. Togawa, Y. Kato, K. Matsubayashi, S. Watanabe, and H. Onimaru. The specific-heat measurement was performed at N-BARD, Hiroshima University. This paper was partly supported by Japan Society for the Promotion of Science KAKENHI Grants No. JP25400375, No. JP16H01073, and No. JP18H04324, and JSPS *Core-to-Core* Program "A Consortium to Exploit Spin Chirality in Advanced Materials."

[1] Y. Togawa, Y. Kousaka, K. Inoue, and J. Kishine, J. Phys. Soc. Jpn. **85**, 112001 (2016), and references therein.
[2] A. Bauer and C. Pfleiderer, *Topological Structures in Ferroic Materials: Domain Walls, Vortices and Skyrmions* (Springer, New York, 2016), p. 1, and references therein.
[3] H. Wilhelm, M. Baenitz, M. Schmidt, U. K. Rößler, A. A. Leonov, and A. N. Bogdanov, Phys. Rev. Lett. **107**, 127203 (2011).
[4] T. Yamashita, R. Miyazaki, Y. Aoki, and S. Ohara, J. Phys. Soc. Jpn. **81**, 034705 (2012).
[5] M. Kakihana, D. Aoki, A. Nakamura, F. Honda, M. Nakashima, Y. Amako, S. Nakamura, T. Sakakibara, M. Hedo, T. Nakama, and Y. Ōnuki, J. Phys. Soc. Jpn. **87**, 023701 (2018).
[6] G. Knebel, R. Boursier, E. Hassinger, G. Lapertot, P. G. Niklowitz, A. Pourret, B. Salce, J. P. Sanchez, I. Sheikin, P. Bonville, H. Harima, and J. Flouquet, J. Phys. Soc. Jpn. **75**, 114709 (2006).
[7] S. Nakatsuji, K. Kuga, Y. Machida, T. Tayama, T. Sakakibara, Y. Karaki, H. Ishimoto, S. Yonezawa, Y. Maeno, E. Pearson, G. G. Lonzarich, L. Balicas, H. Lee, and Z. Fisk, Nat. Phys. **4**, 603 (2008), and references therein.
[8] Y. Muro, Y. Haizaki, M. S. Kim, K. Umeo, H. Tou, M. Sera, and T. Takabatake, Phys. Rev. B **69**, 020401(R) (2004).
[9] J. P. Sanchez and M. M. Abd-Elmeguid, Hyperfine Interact. **128**, 137 (2000), and references therein.
[10] G. R. Stewart, Rev. Mod. Phys. **73**, 797 (2001).
[11] T. Moriya and T. Takimoto, J. Phys. Soc. Jpn. **64**, 960 (1995).
[12] A. J. Millis, Phys. Rev. B **48**, 7183 (1993).
[13] O. Trovarelli, C. Geibel, S. Mederle, C. Langhammer, F. M. Grosche, P. Gegenwart, M. Lang, G. Sparn, and F. Steglich, Phys. Rev. Lett. **85**, 626 (2000).
[14] Y. Matsumoto, S. Nakatsuji, K. Kuga, Y. Karaki, N. Horie, Y. Shimura, T. Sakakibara, A. H. Nevidomskyy, and P. Coleman, Science **331**, 316 (2011).
[15] S. Watanabe and K. Miyake, J. Phys.: Condens. Matter **23**, 094217 (2011).
[16] R. Miyazaki, Y. Aoki, R. Higashinaka, H. Sato, T. Yamashita, and S. Ohara, Phys. Rev. B **86**, 155106 (2012).
[17] S. Ohara, S. Fukuta, K. Ohta, H. Kono, T. Yamashita, Y. Matsumoto, and J. Yamaura, JPS Conf. Proc. **3**, 017016 (2014).
[18] H. Ninomiya, T. Sato, S. Ohara, and K. Inoue, Physica B **536**, 654 (2018).

[19] T. Matsumura, Y. Kita, K. Kubo, Y. Yoshikawa, S. Michimura, T. Inami, Y. Kousaka, K. Inoue, and S. Ohara, J. Phys. Soc. Jpn. **86**, 124702 (2017).
[20] Y. Utsumi, H. Sato, S. Ohara, T. Yamashita, K. Mimura, S. Motonami, K. Shimada, S. Ueda, K. Kobayashi, H. Yamaoka, N. Tsujii, N. Hiraoka, H. Namatame, and M. Taniguchi, Phys. Rev. B **86**, 115114 (2012).
[21] K. Matsubayashi, T. Hirayama, T. Yamashita, S. Ohara, N. Kawamura, M. Mizumaki, N. Ishimatsu, S. Watanabe, K. Kitagawa, and Y. Uwatoko, Phys. Rev. Lett. **114**, 086401 (2015).
[22] K. Umeo, Rev. Sci. Instrum. **87**, 063901 (2016).
[23] S. J. Joshua, Physica A **261**, 135 (1998).
[24] N. Tsujii, H. Kontani, and K. Yoshimura, Phys. Rev. Lett. **94**, 057201 (2005).
[25] V. T. Rajan, Phys. Rev. Lett. **51**, 308 (1983).
[26] J. W. Rasul and A. C. Hewson, J. Phys. C **17**, 2555 (1984).
[27] A. C. Hewson and J. W. Rasul, Phys. Lett. A **92**, 95 (1982).
[28] S. Watanabe and K. Miyake, Phys. Rev. Lett. **105**, 186403 (2010).
[29] V. Laliena, J. Campo, and Y. Kousaka, Phys. Rev. B **94**, 094439 (2016).
[30] K. Tsuruta, M. Mito, H. Deguchi, J. Kishine, Y. Kousaka, J. Akimitsu, and K. Inoue, Phys. Rev. B **93**, 104402 (2016).
[31] A. Bauer, M. Garst, and C. Pfleiderer, Phys. Rev. Lett. **110**, 177207 (2013).
[32] A. N. Bogdanov and D. A. Yablonskii, Sov. Phys. JETP **68**, 101 (1989).